Geoderma 333 (2019) 90–98

Contents lists available at ScienceDirect

Geoderma

journal homepage: www.elsevier.com/locate/geoderma

Structure and hydraulic properties in soils under long-term irrigation with treated wastewater

Frederic Leuther[a,*], Steffen Schlüter[a], Rony Wallach[b], Hans-Jörg Vogel[a,c]

[a] Department of Soil System Sciences, Helmholtz Centre for Environmental Research - UFZ, Theodor-Lieser Str. 4, Halle (Saale) 06120, Germany
[b] Department of Soil and Water Sciences, The Hebrew University of Jerusalem, Rehovot, Israel
[c] Institute of Soil Science and Plant Nutrition, Martin-Luther-University Halle-Wittenberg, Von-Seckendorff-Platz 3, Halle (Saale), Germany

ARTICLE INFO

Handling Editor: Morgan Cristine L.S.

Keywords:
Soil structure
Treated wastewater irrigation
Clay dispersion
Unsaturated hydraulic conductivity
Soil water retention
X-ray microtomography

ABSTRACT

Secondary treated wastewater, a commonly used water resource in agriculture in (semi-)arid areas, often contains salts, sodium, and organic matter which may affect soil structure and hydraulic properties. The main objective of this study was to jointly analyse the effects of long-term irrigation with treated wastewater on physicochemical soil characteristics, soil structure, and soil water dynamics in undisturbed soils. X-ray microtomography was used to determine changes in macro-porosity (> 19 µm), pore size distribution, and pore connectivity of a sandy clay loam and a loamy sand. Differences in the pore network among soils irrigated with treated wastewater, fresh water that replaced treated wastewater, and non-irrigated control plots could be explained by changes in textural composition, soil physicochemical parameters, and hydraulic properties. In this study we showed that irrigation led to the development of a connected macro-pore network, independent of the studied water quality. The leaching of silt and clay particles in the sandy soil due to treated wastewater irrigation resulted in an increase of pores < 130 µm. While this change in texture reduced water retention, the unsaturated hydraulic conductivity was diminished by physicochemical alteration, i.e. induced water repellency and clay mineral swelling. Overall, the fine textured sandy clay loam was much more resistant to soil alteration by treated wastewater irrigation than the loamy sand.

1. Introduction

The utilization of treated wastewater (TWW) has become an important source of irrigation water in many countries, primarily in arid and semiarid areas where water scarcity is severe. In Israel, already 75 % of wastewater is treated and re-used for irrigation, covering 50 % of the water consumption in agriculture (OECD, 2015). Compared to fresh water (FW), TWW is generally characterized by a higher load of dissolved organic matter, suspended solids, sodium adsorption ratio, and considerable levels of salinity. Therefore, irrigation with TWW can increase salinity and sodicity of soils at depths down to 1.5 m (Lado and Ben-Hur, 2009; Levy, 2011; Bedbabis et al., 2014), accompanied with clay migration due to dispersion of clay minerals in the top soil (Bardhan et al., 2016). The latter can enhance soil sealing, reduce infiltration, increase soil loss in sandy soils, and enhance slaking in clay soils (Lado et al., 2005).

At the same time, higher loads of organic matter in the effluents are reported to result in inconsistent effects on the carbon concentrations of the topsoil. While in some soils the organic carbon concentrations were increased (Jueschke et al., 2008), in others the effect was marginal (Lado et al., 2012) or it was reduced by priming effects due to the stimulation of microbial activity (Adrover et al., 2012). It is well known that soil structure is to a large extent formed by soil biota (Oades, 1993) and that the quality and quantity of organic matter in irrigation water can shape the structure of soil biological communities (Adrover et al., 2012; Frenk et al., 2014; Ibekwe et al., 2018). Hence, organic compounds introduced through TWW irrigation are expected to affect soil structure and thereby soil water dynamics.

Lado and Ben-Hur (2009) and Levy (2011) reported that TWW irrigation decreased soil structural stability and significantly altered soil pore architecture. This resulted in a reduction in saturated hydraulic conductivity in clay and loamy soils due to clogging of the pores with suspended solids while sandy soils were not affected. Bardhan et al. (2016) reported that the conductivity of clay soil was reduced in a water potential range of 0 down to −100 hPa, suggesting that the volume fraction of macro- and meso-pores were affected by pore narrowing through dissolved organic matter that may have led to enhanced clay swelling. Halliwell et al. (2001) hypothesized that changes in the

* Corresponding author.
E-mail address: frederic.leuther@ufz.de (F. Leuther).

https://doi.org/10.1016/j.geoderma.2018.07.015
Received 7 March 2018; Received in revised form 11 June 2018; Accepted 8 July 2018
Available online 19 July 2018

pore system of the soil due to TWW seem to be the dominant factor for the reduction in soil hydraulic conductivity. Moreover, it has been shown that TWW contains hydrophobic compounds which can cause water repellency and can effect soil water dynamics such as reduced infiltration capacity, overland flow, formation of preferential flow path, and reduced water retention (Bauters et al., 2000; Diamantopoulos et al., 2013; Wallach and Jortzick, 2008). For the loamy sand soil discussed in this paper, an impact of reduced wettabiliy on the stability of water infiltration and the occurrence of preferential flow has been confirmed by heterogeneous water distributions in the field (Rahav et al., 2017) and infiltration experiments in undisturbed soil columns (Leuther et al., 2018).

The main objective of this study was to jointly analyse the effects of long-term irrigation with TWW on soil structure and soil water dynamics in undisturbed soils which integrates effects of changes in microbial communities, clay mineral swelling and dispersion, clogging of pores, and induced water repellency by loads of organics, suspended solids, and sodium. We used X-ray microtomography to determine the undisturbed macro-pore network of a sandy clay loam and a loamy sand irrigated with TWW for more than 7 years. The measurements were concentrated on the topsoil, assuming that this is the most affected region under drip irrigation (Assouline and Narkis, 2011; Elifantz et al., 2011; Wallach et al., 2005). Furthermore, we determined differences in soil texture and physicochemical characteristics to analyse how TWW irrigation potentially had changed clay content, and analysed the effect on soil hydraulic properties as integrative soil characteristics reflecting changes in soil wettability, soil texture, and soil structure.

2. Materials & methods

2.1. Study sites and soil sampling

The topsoils of two commercial orchards located in the coastal plain of Israel were investigated. The region is dominated by Lovisols (Singer, 2007) of a sandy texture and has two pronounced climate seasons, a hot and dry summer where orchards are irrigated, and a rainy winter without irrigation. At the study sites, water was applied via drip irrigation and the amount was adjusted to the daily evapotranspiration rates, approximately 700 mm per dry season. Soil cultivation was mainly inorganic fertilization without any tillage. To capture seasonal dynamics due to the irrigation schemes, the sampling was carried out in October 2015 and February 2016. We investigated the top soil (0 to 200 mm depth) of a loamy sand close to Rehovot (31°53'59.0"N, 34°51'00.0"E), denoted in the following as S, and a sandy clay loam close to Hadera (32°24'48.0"N, 34°58'02.3"E), denoted as L.

For the S-site, the water management was changed from fresh water (FW) to secondary treated wastewater irrigation (TWW) in 2008. In 2012, single plots of a block design experiment were converted back to FW irrigation for soil reclamation (Rahav et al., 2017). For the L-site, farmers have used secondary treated wastewater for more than 30 years. Soil samples were randomly taken within the wet soil along the dripper lines (FW and TWW) and between the tree rows beyond the reach of irrigation water (NoI) as a control for untreated soil. The study sites enclosed an area of 4500 m^2 at the S-site and of 1500 m^2 at the L-site. The chemical properties of the different water treatments are given in Table 1.

Cylindrical polycarbonate containers with a wall thickness of 3 mm and an outer diameter of 100 mm were used for soil sampling. These had a height of either 100 mm or 200 mm, depending on the feasibility of undisturbed sampling in the presence of woody roots below the trees. Soil samples were excavated by using a sampling device for undisturbed soil cores manufactured by UGT GmbH, Germany (Kuka et al., 2013). The method is adapted from an excavation technology for large soil monoliths, where surrounding soil is pre-cut and continuously removed by a rotating cutting sleeve. While slowly penetrating the soil, the remaining, undisturbed soil core is taken in by a sampling cylinder placed inside the sleeve. All samples were immediately covered with a lid, stored in plastic bags to keep them field moist, carefully packed and shipped to Germany. Overall, 17 soil cores (3 S-FW, 4 S-NoI, 3 S-TWW, 7 L-TWW) were taken in October 2015 and 26 soil cores (6 S-FW, 2 S-NoI, 6 S-TWW, 5 L-TWW, 7 L-NoI) in February 2016. Additional 77 undisturbed samples (50 mm in diameter and 50 mm in height) were taken from the topsoil in the vicinity of larger soil cores to measure soil water repellency.

Table 1
Irrigation water characteristics (EC = electrical conductivity, SAR = sodium absorption ratio) for the two study sites (S = loamy sand, L = sandy clay loam, FW = fresh water, TWW = treated wastewater): mean values based on two measurements in 2014 and 2015 (S-site adapted from Rahav et al., 2017).

Site	pH	EC	SAR	*Na*	*Ca*	*Mg*
		[dS m^{-1}]	[(meq/L)$^{0.5}$]	[mg L^{-1}]	[mg L^{-1}]	[mg L^{-1}]
S-FW		0.77	1.73	65.32	61.00	28.31
S-TWW	7.2	1.65	4.61	164.68	61.80	21.02
L-TWW	7.4	1.32	3.96	153.00	85.00	16.80
	Cl [mg L^{-1}]	$NO_3 - N$ [mg L^{-1}]	$NH_4 - N$ [mg L^{-1}]	SO_4 [mg L^{-1}]	*P* [mg L^{-1}]	*K* [mg L^{-1}]
S-FW	108.20	< 1.50	0.63	253.92	< 0.01	3.58
S-TWW	231.60	< 1.50	53.82	487.20	7.38	26.00
L-TWW	175.50	2.26	8.32	369.50	5.20	22.10

2.2. Soil properties

The total carbon (C) and nitrogen (N) concentrations in air dried soil were measured for each sample. To exclude a possible impact of carbonates on the measured C values, the soil was tested for lime content via hydrochlorid acid (10%) with a negative result (Jahn et al., 2006). C and N were determined by elemental analysis using gas chromatography (Vario EL Cube, Elementar). Three replicates per sample were ground, weighed (60 mg) and burned at 950 °C.

Particle size distribution in mineral soil was analysed by sedimentation following DIN ISO 11277 (2002). Samples had been dried in an oven at 105 °C, and separated from carbonates and organic substances before sedimentation.

Three different parameters were determined to describe changes in soil chemical properties by TWW irrigation: acidity (pH), electrical conductivity (EC), and sodium adsorption ratio (SAR) following the protocol described by Rowell (1994). Oven dried soil samples were mixed and sub-samples of 10 g were suspended in 25 mL distilled water and shaken for 15 min to measure soil pH_{H2O} in a 1:2.5 suspension with a pH meter. The pH was recorded after 1 min time of stabilization. Afterwards, 25 mL more distilled water was added, the reagent was shaken for 30 min, and the EC was measured in the supernatant of the 1:5 suspension. By multiplication with a factor of 6.4, the measured value was converted to EC of a saturation extract, the reference water content to describe soil salinity (Rowell, 1994). After filtering the extraction (Whatman No.1), Na^+, Ca^{2+}, and Mg^{2+}-ion concentrations were analysed via ion chromatography (DIONEX Aquion, Thermo Fisher). The SAR was determined via

$$SAR = \frac{Na^+}{\sqrt{\frac{(Ca^{2+} + Mg^{2+})}{2}}}, \quad (1)$$

all concentrations were expressed in millimol per kilogram.

Soil water repellency at soil surface was determined by two methods, the water drop penetration time test (WDPT) (Doerr, 1998) and the sesille drop contact angle (CA) (Bachmann et al., 2000). Therefore, additional soil samples were placed in an oven at 50 °C until a reference water content corresponding to that of air dried soil was reached. The WDPT was determined by placing three drops of 50 µL

distilled water on the soil surface and recording the required time to their complete infiltration. The initial contact angle of a 15 µL-water drop was measured with a goniometer (EasyDrop DSA20E, KRÜSS GmbH, Germany) for a flat single-grain of air dried, sieved soil.

2.3. Soil structure analysis via X-ray microtomography

All samples were scanned using an X-ray microtomograph (X-TEK XT H 225, Nikon Metrology) to capture the undisturbed soil structure. The samples were scanned with energy settings of 140 kV and 470 µA, and a 1.5 mm copper filter to reduce beam hardening artefacts and prevent overexposure at the lateral margins of the detector panel. The exposure time for each image was 1000 ms with two frames per projection and a total of 2748 projections. The reconstruction of three-dimensional images was done with the CT Pro 3-D software package (version 3.1) at a spatial resolution of 60 µm. Four additional subsamples (30 mm in height and in diameter) of each irrigation treatment were taken from the midst of the large 100 mm soil cores and scanned at a resolution of 19 µm to widen the spatial scale of structure analysis. Here, a 0.1 mm copper filter was used and the energy settings were changed to 115 kV and 170 µA.

Image processing and analysis were done with the open source software packages QuantIm (Vogel et al., 2008) and Fiji ImageJ V. 1.50d (Schindelin et al., 2012) and mainly followed the workflow described by Schlüter et al. (2016). At first the raw image volumes were filtered with a 2D-Nonlocal Means filter from every dimension (x, y, and z) to reduce image noise equally in all directions. Second, the images were corrected for vertical differences in average image intensity due to shading and cone beam artefacts. Third, images were segmented into three classes: pore system, particulate organic material, and soil matrix, following Schlüter et al. (2014).

Macro-porosity, here defined as the CT derived porosity, and the amount of particulate organic material (> 2 voxels), such as roots and litter, were determined as the ratio of segmented voxels to total number of voxels within the sample. The segmented pore network was analysed in terms of change in porosity over sample depth, pore size distribution, and connectivity. The pore size distribution was determined with the maximum inscribed sphere method in the BoneJ plugin for Fiji ImageJ (Doube et al., 2010). The pore size distribution of every sample was classified in one-voxel increments. This allowed to combine the pore sizes determined at different resolution (Vogel et al., 2010). The connectivity of the pore network was defined by their Γ-indicator (Eq. (2)), reflecting the probability of two randomly chosen pore voxels to belong to the same pore cluster (Renard and Allard, 2013).

$$\Gamma(p) = \frac{1}{n_p^2} \sum_{i=1}^{N(X_p)} n_i^2 \quad (2)$$

Here, n_p is the total number of pore voxels in the analysed volume X_p and n_i is the number of voxels per cluster. Therefore, $\Gamma(p)$ is dominated by the proportion of pores which are connected to the biggest pore cluster. Overall, the undisturbed pore networks were analysed for 23 S-samples (8 × FW, 9 × TWW, 6 × NoI), 15 L-samples (9 × TWW, 6 × NoI), and 10 sub-samples (4 × S-FW, 4 × S-TWW, 2 × L-TWW). The top soil (0 to 10 cm) was analysed for all samples while for the depth between 10 and 20 cm this was possible only for three replicates from the L-NoI and L-TWW plots, respectively.

2.4. Soil hydraulic properties

The soil water retention curve (SWRC) and unsaturated hydraulic conductivity were measured with the HYPROP device for larger soil cores (METER Group, Inc. USA) for a potential range from 0 to −5000 hPa using the evaporation method developed by Schindler et al. (2010). For the dry end of the SWRC (< − 10 000 hPa), soil water retention was determined with a WP4C (METER Group, Inc. USA). For hydraulic conductivity close to saturation the evaporation method is limited, therefore, the measurements were supplemented by Multi-Step-Flux experiments for a potential range from − 2 to −35 hPa (Weller and Vogel, 2012). To prevent changes in soil chemistry and structure during the experiment, the salt concentrations of the irrigation water were adapted to the field specific water characteristics. At the end of the experiments, soil samples were dried at 105 °C to determine bulk density, total porosity, and saturated water content.

2.5. Statistical analysis

The comparisons of means for each soil property were done by analysing the variance of each treatment (ANOVA) using the lsmeans package in R Version 3.4.2 (Lenth, 2016). Parameters were tested for equality of variances with Levene's test for homogeneity of variance and the means were compared by Tukey's multiple comparison of means based on a 95% family-wise confidence level. Furthermore, the multivariate regression method Partial Least Squares Regression (PLSR) implemented in the pls package in R Version 2.6-0 (Mevik and Wehrens, 2007) was used as an exploratory analysis tool to select suitable predictor variables for soil hydraulic properties. Therefore, the physico-chemical and textural soil properties were grouped into texture, water repellency, and salinity. These were used as predictor variables for soil water retention and hydraulic conductivity at field capacity (water potential −100 hPa). Finally, a combination of the potential most influential parameter according to literature were tested for its predictive power (sand concentration, SAR, and initial contact angle at soil surface). All predictors were tested for cross-validation by leave-one-out cross-validation.

3. Results and discussion

3.1. Soil properties

According to FAO classification, all treatments at the S-site were classified as loamy sand and at the L-site as sandy clay loam (Table 2, Fig. S1 in the supplementary material (s.m.)). For both locations, no significant differences in soil texture were found between non-treated NoI and irrigated topsoil due to high variations within the treatments. Nevertheless, at the S-site a significant increase in sand content was determined for the S-TWW soil compared to S-FW ($p = 0.02$) most likely caused by eluviation of silt and clay particles. For the L-soil, no differences in soil texture classes between the TWW irrigated and the non-irrigated treatments were found.

TWW had an effect on soil acidity (pH) and salinity (EC) in the sandy S-soil but not in loamy L-soil, where pH remained around 7.5 and EC around 1.5 dS m^{-1} for both treatments. Soil pH under S-FW irrigation (pH 7.2) was slightly reduced compared to non-treated soil (pH 7.4), but under TWW irrigation the soil was significantly acidified to a mean pH of 5.7 ($p < 0.001$). Compared to the control, a significant increase in soil salinity occurred in both irrigation treatments. Soil sodicity was affected most. In both textures the SAR ratios were the greatest for TWW plots, yet with considerable variations in the S-TWW treatment. Also, some S-FW samples showed an increased sodium content compared to the non-irrigated treatments. The inequality in variance of the measured SAR values within the single treatments prevented a statistical analysis.

Due to their high variances, both the total carbon and nitrogen concentrations of the S-soil were not significantly different below drip-irrigation compared to the non-irrigated plot. In contrast, for the L-soil, both the total carbon and nitrogen concentrations of the NoI-samples were significantly increased compared to TWW irrigation ($p = 0.05$). The C/N ratio was around 9:1 for all samples, independent of the location and the irrigation regime.

All sampling locations except for the S-NoI were classified as subcritical water repellent (35° < CA < 90°) to water repellent (CA ≥ 90°).

Table 2
Study sites characteristics (S = loamy sand, L = sandy clay loam and treatments: NoI = non-irrigated control, FW = fresh water, TWW = treated wastewater): grain size distribution, chemical soil parameters (EC = electrical conductivity, SAR = sodium absorption ratio), total carbon (C) and nitrogen (N) concentrations, and water repellency characteristics (CA = initial contact angle, WDPT = water drop penetration time). Values in parentheses are the standard errors.

Parameter	S-NoI (n = 4)	S-FW (n = 9)	S-TWW (n = 9)	L-NoI (n = 6)	L-TWW (n = 9)
Sand [g 100 g^{-1}]	81.4 (2.0)	79.1 (2.1)	86.1 (1.6)	65.5 (2.3)	63.8 (0.7)
Silt [g 100 g^{-1}]	7.8 (0.9)	9.0 (1.0)	5.7 (0.6)	12.6 (0.2)	14.6 (0.7)
Clay [g 100 g^{-1}]	10.8 (1.2)	11.9 (1.2)	8.2 (1.1)	21.8 (2.0)	21.6 (0.9)
Bulk density [g cm^{-3}]	1.64 (0.02)	1.31 (0.04)	1.32 (0.06)	1.48 (0.03)	1.48 (0.03)
pH [-]	7.4 (0.1)	7.2 (0.1)	5.7 (0.2)	7.5 (0.1)	7.6 (0.1)
SAR	0.6 (0.1)	1.4 (0.2)	2.7 (0.3)	0.5 (0.0)	3.6 (0.1)
EC [dS m^{-1}]	0.9 (0.1)	1.7 (0.2)	2.0 (0.2)	1.6 (0.1)	1.4 (0.1)
C_{tot} [g 100 g^{-1}]	0.55 (0.08)	1.18 (0.19)	1.21 (0.17)	1.74 (0.33)	0.83 (0.09)
N_{tot} [g 100 g^{-1}]	0.07 (0.01)	0.13 (0.02)	0.13 (0.02)	0.17 (0.03)	0.10 (0.01)
C/N-ratio	8.28 (0.51)	9.18 (0.32)	8.96 (0.34)	9.96 (0.49)	8.54 (0.32)
CA [°]	NaN	69.3 (3.6)	91.1 (2.3)	113.3 (3.2)	48.8 (7.3)
WDPT [s]	0 (0)	41.4 (20.4)	144.9 (71.8)	882.8 (190.1)	12.4 (2.7)

Both water repellency characteristics, WDPT and CA, were significantly greater in S-TWW compared to S-FW and S-NoI as reported in detail by Leuther et al. (2018). For the L-soil, the surfaces of L-NoI samples were classified as strongly to severely water repellent by WDPT, while L-TWW samples were classified as wettable to slightly water repellent.

In summary, changes in physicochemical soil properties due to long-term irrigation with TWW were mostly found for the S-soil. Here, changes in pH and SAR were highly significant, while increase in carbon content and electrical conductivity, in combination with slight changes in textural composition were also found in FW irrigated plots. Due to high evaporation in summer, the low salt contents of the fresh water can still increase salinity in top soil. Furthermore, 3 years of TWW application prior to FW could have affected the soil as well. This might explain the high variance in SAR and the reduced wettability. Although sodicity increased in TWW plots, soils in all treatments from both sites can be classified as non-salt affected, with EC < 4.0 dS m^{-1} and SAR < 6 (meq/kg)$^{0.5}$ (Rengasamy, 2010).

Thirty years of TWW irrigation on the L-soil did not change soil texture, pH, and EC. It seems that the annual precipitation was sufficient to prevent an increase in total salinity but not for Na accumulation. The greater C and N concentrations in the L-NoI control might be explained by the observed accumulation of organic litter and reduced biological decomposition during dry summers. For S-NoI, no litter accumulation was observed.

Except for acidification of S-TWW, all measured changes in soil properties were in agreement with previous studies on TWW effects with similar soil textures (Lado et al., 2012; Tarchouna et al., 2010; Schacht and Marschner, 2015). While most studies reported that soil pH increased with TWW irrigation due to accumulation of alkalis, here, pH dropped significantly. Similar, but less intense reductions in pH were also reported by Bedbabis et al. (2014). In both studies ammonium dominated the nitrogen supply in irrigation water, which can cause soil acidification due to ammonium uptake by plants and microbial nitrification (Marschner et al., 1986). Due to the low amount of silt in the S-soil, the pH buffer capacity was reduced compared to the L-soil.

Differences in soil carbon and nitrogen concentrations due to a priming effect or due to higher loads of organics by TWW could not be detected due to high variability within the treatments. The narrow C/N-ratio of 9:1 was found for all treatments which is close to the ratio of citrus leaves (Pedrero et al., 2010). This indicates that the carbon and nitrogen storage in the soils was dominated by the input and accumulation of organic litter from the trees and not by the quality of irrigation water.

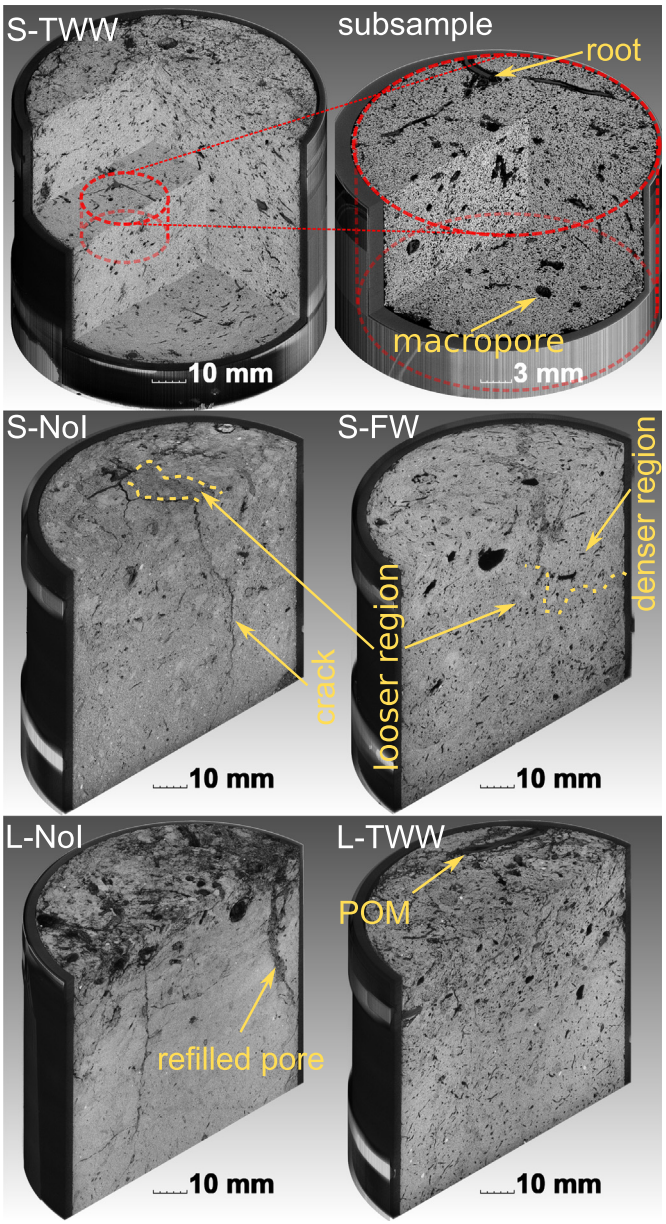

Fig. 1. Reconstructed X-ray microtomography images of the topsoil (sites: S = loamy sand, L = sandy clay loam and treatments: NoI = non-irrigated control, FW = fresh water, TWW = treated wastewater) at a spatial resolution of 60 µm and one subsample (top right, 19 µm) before image processing. Grey values are related to material densities where black represents pores, dark grey: organics, and light grey to white: soil matrix.

3.2. Soil structure

The soil structure of a representative 10 cm sample of every treatment and one 3 cm sub-sample is shown in Fig. 1 to provide a visual impression of the structural heterogeneities. This heterogeneity manifests itself by looser and denser regions, refilled pores, cracks, small

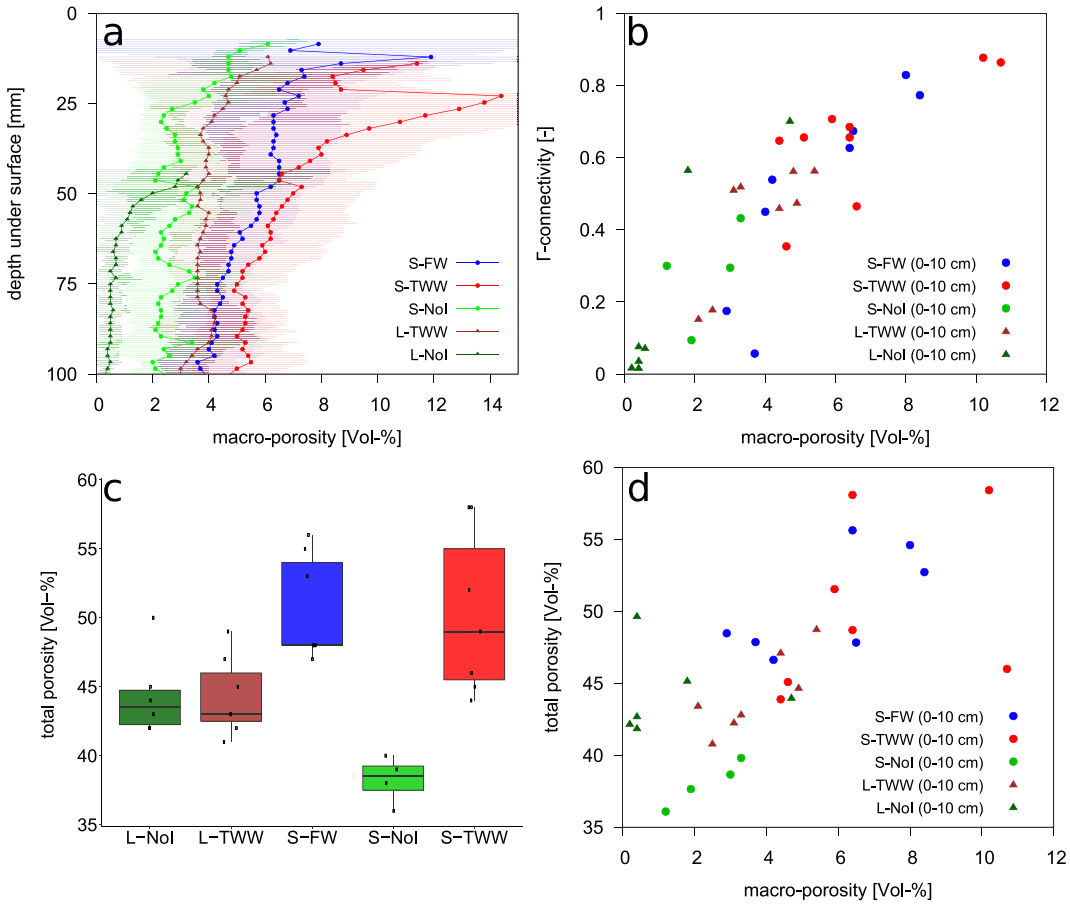

Fig. 2. Pore network characteristics (sites: S = loamy sand, L = sandy clay loam and treatments: NoI = non-irrigated control, FW = fresh water, TWW = treated wastewater) determined at a resolution of 60 µm (a,b), and total porosity determined by dry weight (c). The depth profile (a) shows the mean macro-porosities and the shaded area margins the 95% confidence interval of the mean determined by two times standard deviation.

stones, roots and particulate organic matter distributed over the samples (for details on POM abundance and distribution see Fig. S2, s.m.). Fig. 2 shows the depth profiles of the averaged macro-porosities (pores > 60 µm) for every treatment (a), their macro-pore connectivity (b), total porosity determined by dry weight (c), and total porosity as a function of macro-porosity (d). The visible macro-porosity of the different S-treatments decreased with depth while for the L-soil the depth profiles were more uniform. A significant increase in macro-porosity due to irrigation (FW and TWW) was determined for the sandy S-soil, but not for the more loamy L-soil. The Γ-connectivity of the pore network increased with increasing macro-porosity due to connected biopores. For the S-soil, macro-porosity (> 60 µm) contributed 11% to the total soil porosity, and only 6% for the L-soil. Thus, the relations between macro-porosity and total porosity were different for the two orchards. While for the S-treatments, the visible macro-porosity had a strong influence on the total porosity (R^2 = 0.52), for the L-soil the total porosity did not change by increasing macro-porosity (R^2 = 0.08). The scatter plots also reveal the great heterogeneity within the treatments. Therefore, no significant differences in macro-porosity, connectivity or total porosity were determined between S-FW/S-TWW and L-NoI/L-TWW. Nevertheless, S-soil was significantly loosened ($p < 0.01$) in the irrigated area from S-NoI: 38.1 vol.% total porosity to S-FW: 50.5 vol.% and to S-TWW: 50.3 vol.%, while for the L-soil the mean bulk density did not change between the treatments, and remained at 44.3 vol.%. To determine specific changes inside the pore systems, a detailed look into the distribution of different pore sizes was necessary.

The averaged pore size distributions (PSD) for pores larger than 60 µm are depicted in Fig. 3a) for the S-soil and in b) for the L-soil. The second row provides the PSD of the smaller sub-samples for pores larger than 19 µm (c) and the combined cumulative porosity after merging both scales (d). The grey background marks the range, where pores smaller than 4 voxels are expected to be systematically underestimated due to image processing (Vogel et al., 2010). The high resolution of the sub-samples expands the range of valid data from secondary pores (biopores) down to primary pores arising from the arrangement of soil particles. For both soils, the rise in macro-porosity under irrigation (FW and TWW) was distributed over a wide spectrum of pore sizes from 90 to 1700 µm, and was the largest in a pore diameter range of 210 to 1000 µm. For the L-soil, within the different treatments no differences in PSD were determined between the two sampling depths (0 to 10 cm and 10 to 20 cm). Pores smaller than 130 µm, as detected by the sub-samples at higher resolution, were more abundant in the TWW irrigated S-soil resulting in greater cumulative macro-porosity.

TWW irrigation reduced the clay and silt content for S-soil (Table 2), hence, more intergranular spaces were detected as pores instead of the embedding matrix of fines. Fig. 4 shows two representative slices of the reconstructed X-ray microtomographies of a S-FW sub-sample (left side) and a S-TWW sub-sample (right side). For both treatments, we enlarged a section of the image to demonstrate the discussed differences in segmented pore classes, especially for pores smaller than 130 µm. Most sand grains of the S-FW sample were embedded in a fine textured material, whereas for S-TWW, the sand grains were surrounded by pores.

In summary, it has been hypothesised that TWW irrigation could lead to a reduction of porosity due to enhanced clay swelling, organic coatings on pore walls, or pore clogging through suspension and translocation of clay particles and suspended solids in the wastewater.

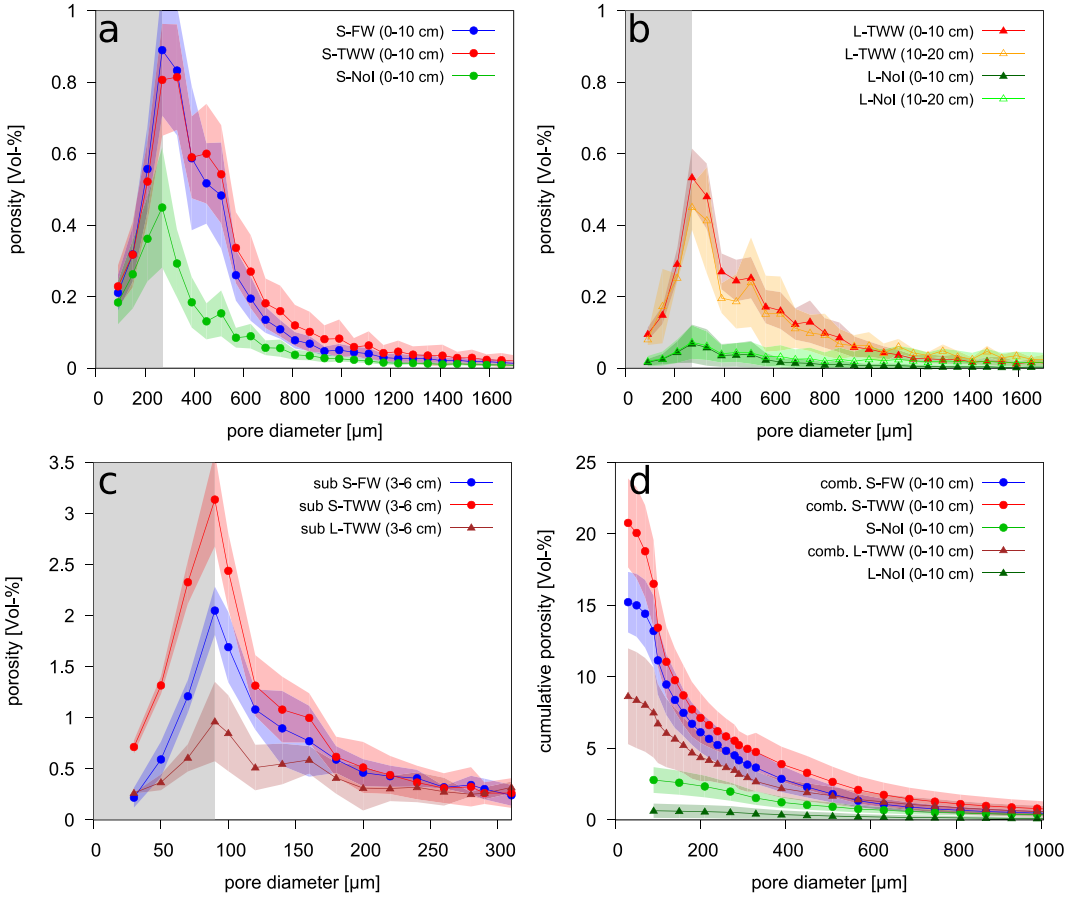

Fig. 3. Mean distribution of classified pore sizes for loamy sand (NoI = non-irrigated control, FW = fresh water, TWW = treated wastewater) of the top soil (a), for sandy clay loam at two depths (0 to 10 cm and 10 to 20 cm, b), and for the sub-samples (c). The grey background marks the range of uncertainty of the detection method, the shaded area of the lines margins two times standard error. The cumulative porosity based on 10 cm samples, which was combined with sub-samples porosity (comb.) for S-FW, S-TWW, and L-TWW.

These parameters are well below our detection limit, but could have caused a shift of the pore size distribution towards smaller pores between S-TWW and S-FW, and between L-TWW 0 to 10 cm and L-TWW 10 to 20 cm respectively. In our study, neither the total porosity nor the visible macro-porosity indicated that the pore system was negatively affected by TWW irrigation. On the contrary, the macro-porosity was increased in terms of quantity and connectivity in the irrigated plots. This might be due to greater root activity, or due to soil fauna which was not limited by drought or nutrients. The higher resolution of the sub-samples enabled the detection of an increased macro-porosity for S-TWW, which might have been due to the loss of clay minerals previously filling the pores between the sand grains and by a greater density of fine roots.

Overall, for the S-soil the visible macro-porosity was positively correlated with total porosity and with their connectivity. This indicates that the micro- and meso-porosity was not affected by TWW compared to FW irrigation. For the L-soil, no significant differences were determined between the treatments in terms of porosity, macro-porosity,

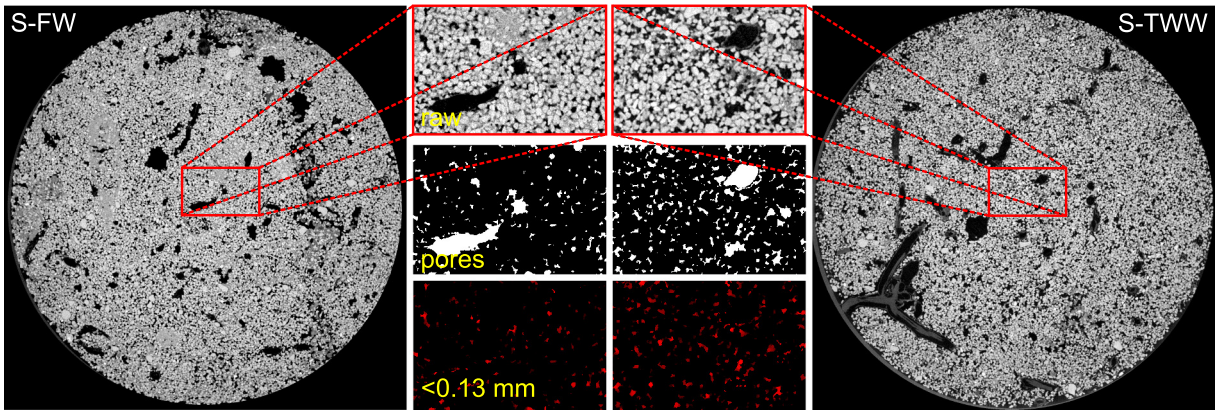

Fig. 4. Raw X-ray microtomography images of a fresh water (S-FW) and treated wastewater (S-TWW) irrigated loamy sand sub-sample at a certain depth. The enlarged details of the pictures depict the segmented pore spectrum and pores smaller than 13 µm.

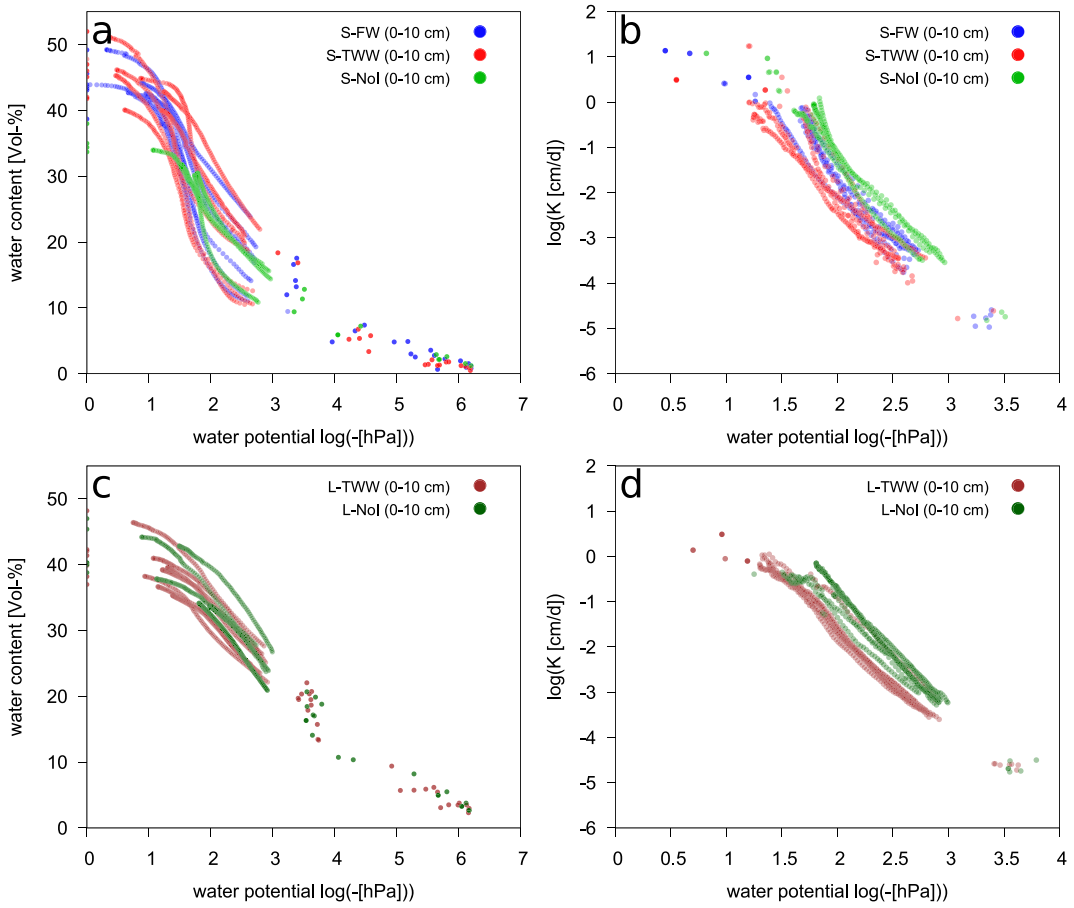

Fig. 5. Soil water retention curve (SWRC) and hydraulic conductivity (sites: S = loamy sand, L = sandy clay loam and treatments: NoI = non-irrigated control, FW = fresh water, TWW = treated wastewater). Data points for SWRC were determined by HYPROP (< log(−−4.5 hPa)) and WP4C (> log(−−4.5 hPa)), for hydraulic conductivity by Multi-Step-Flux (< log(−−1.5 hPa)) and HYPROP (> log(−−1.4 hPa)) experiments.

Table 3
Results of a Partial Least Squares Regression analysis. Percentage of the variance in water content/hydraulic conductivity at −100 hPa explained by different predictor variables (EC = electrical conductivity, SAR = sodium absorption ratio, WDPT = water drop penetration time, CA = initial contact angle) for all samples and separated for both locations (S = loamy sand, L = sandy clay loam).

Water content at −100 hPa	All samples	S-samples	L-samples
Predictor variables:			
Texture: sand & clay	68.72%	28.45%	12.07%
Water repellency: WDPT & CA	25.84%	9.13%	2.78%
Salt: SAR & EC	2.49%	1.00%	1.00%
Combined: sand & SAR & CA	70.93%	32.60%	21.40%
Hydraulic conductivity at −100 hPa			
Predictor variables:			
Texture: sand & clay	17.48%	5.47%	32.48%
Water repellency: WDPT & CA	50.69%	22.23%	64.41%
Salt: SAR & EC	25.90%	33.81%	44.29%
Combined: sand & SAR & CA	43.43%	10.84%	87.25%

or connectivity. At both orchards, macro-porosity and visible POM were an important component of soil structure, mainly in 0 to 6 cm depth, and therefore might influence soil water dynamics.

3.3. Soil hydraulic properties

For the S-soil (Fig. 5a), water retention curves varied considerably with a tendency of steeper slopes (i.e. earlier drainage) in S-TWW samples. The unsaturated hydraulic conductivities (b) were greater in S-NoI samples which was consistent with a lower volume fraction of macro-pores derived by CT which were air filled at low water potentials. For the L-soil (c), water retention curves had similar slopes for both treatments. Differences in soil water content between −10 hPa and −100 hPa were caused by different saturated water contents due to differences in porosity. The unsaturated hydraulic conductivities were not significantly different between both treatments (d).

According to Young-Laplace equation, the pore spectrum analysed via image analysis was drained at water potentials between 0 and −50 hPa for the large samples and −158 hPa for the sub-samples. The differences in visible macro-porosity were therefore represented by the variance of the SWRCs close to saturation, but the highly sensitive range around −100 hPa was not covered for all treatments. Nevertheless, sub-samples of the S-soil indicated the loss of clay as an explanation for differences in the cumulative macro-porosity between S-FW and S-TWW (Fig. 3). Furthermore, a fast draining SWRC is typical for sandy soils.

To determine the sensitivity of hydraulic properties towards textural composition and physicochemical soil properties, their correlations with water contents at −100 hPa and their respective hydraulic conductivities were evaluated via Partial Least Squares Regression. In Table 3 we list the percentages of explained variability in the dependent variable by a set of predictors lumped into texture, water repellency, and salinity. Finally we combined the most influential parameters as a set of predictors. The highest predictive power was found by including all samples for model calibration due to salient differences in hydraulic properties between the study sites. Also the predictive power for the hydraulic conductivity of L-samples was high due to low variability

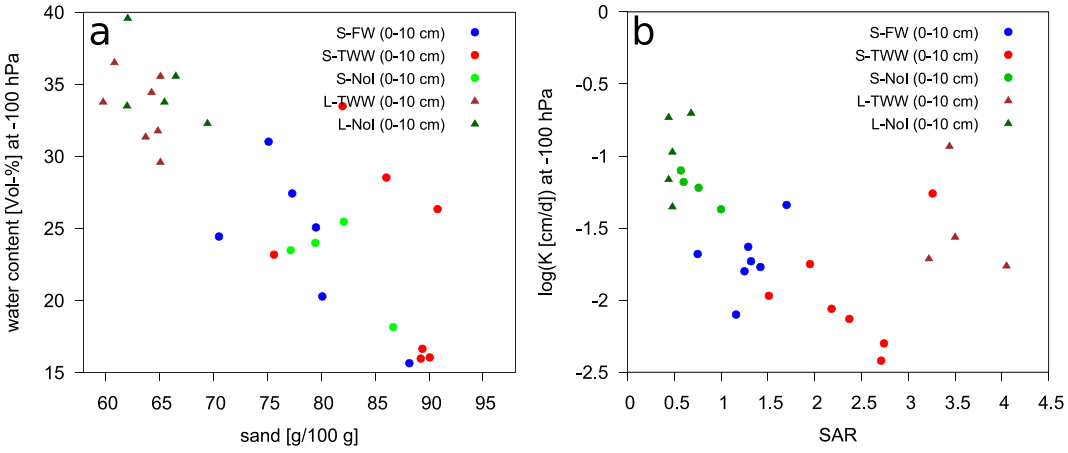

Fig. 6. Water content and hydraulic conductivity (k) at −100 hPa (sites: S = loamy sand, L = sandy clay loam and treatments: NoI = non-irrigated control, FW = fresh water, TWW = treated wastewater).

within the samples. The predictive power of the determined parameters was weak for the S-soil due to high variances.

For water retention at −100 hPa, soil texture was the best predictor. Considering all samples, variances in sand and clay content explained 69% of the variability in water retention, but this was found to be weak when only looking at the samples from one specific site (Fig. 6a). Yet, the eluviation of fines may explain the overall lower water retention at −100 hPa. Using the sand content to predict the hydraulic conductivity at −100 hPa did not result in a comparatively good prediction. Here, water repellency and SAR provided the best predictive powers. The conductivity for the S-soil decreased with increasing concentration of sodium (Fig. 6b). Also the conductivity of the L-soil was reduced by SAR, but not that drastically. This could be an indicator that sodium had caused enhanced soil swelling and pore clogging by clay migration in the TWW-treatments, which was below the detection limit by microtomography.

Causes of reduced hydraulic conductivity by TWW were reported to be related to entrapment of suspended solids originating from the TWW and decreased pore size distribution by adsorption of soluble organic molecules on soil particles (Lado and Ben-Hur, 2010). However, the effect of reduced hydraulic conductivity was mostly related to fine-textured soils and in most cases only the saturated hydraulic conductivity was considered which is highly sensitive to macro-pore flow. Our analysis of soil structure showed that the macro-porosity of the S-soil covered 30 to 40% of the total porosity and the major differences were detected for small pores. Hence, significant differences in saturated hydraulic conductivity for the S-soil are not expected. For unsaturated field conditions, we could show that TWW irrigation reduced the unsaturated hydraulic conductivity.

In summary, both parameters, sand content and SAR, did explain some variability of differences in water retention and unsaturated hydraulic conductivities. Nevertheless, outliers were found in both cases, especially for the S-soil. Besides textural compositions, other parameters can influence hydraulic properties, such as organic material, macro-pore-flow, swelling and shrinking, and reduced wettability.

4. Conclusion

Long-term irrigation with secondary treated wastewater (TWW) proved to have different effects on physicochemical characteristics of the topsoil. Seven years of TWW irrigation on a loamy sand already changed soil textural composition, acidity, salinity, and SAR, while 30 years of TWW irrigation on a sandy clay loam only increased the SAR of the soil. For both soils, organic carbon and nitrogen contents were mainly influenced by the accumulation of litter from the trees and not by the quality of irrigation water. By analysing the macro-pore network (> 60 µm) it was shown that irrigation in general promoted the development of a macro-pore system in terms of volume and connectivity. No constriction of the macro- and meso-pores due to enhanced clay swelling or organic coatings was detected. On the contrary, for the loamy sand an increase of porosity by TWW compared to the replacing fresh water irrigation was detected due to the eluviation of dispersed clay minerals, which was reflected by a reduced soil water retention and greater visible porosity (> 19 µm). The well developed macro-pore networks might promote water flow close to saturation, but when unsaturated, a reduction in hydraulic conductivity was found for both soils, suggesting that mainly primary pores and small macro-pores were affected by TWW irrigation. These small-scale changes in hydraulic properties might exacerbate instabilities in water infiltration promoting the formation of preferential flow. With regard to the long history of TWW application on the more fine textured soil, the detected changes for the top soil were marginal.

Acknowledgements

This work was supported by the German Federal Ministry of Food and Agriculture (FKZ: 2813IL04) and partially by the Israel Ministry of Agriculture. It is part of the project “Impact of effluent irrigation on soil water dynamics and sustainable land use: Synergistic effects of altered soil structure and wettablility”. We thank G. Lerner for his help during field work, B. Apelt and Dr. M. Köhne for the laboratory work, and Dr. Mick Wu for the statistical consultation.

Appendix A. Supplementary data

Supplementary data to this article can be found online at https://doi.org/10.1016/j.geoderma.2018.07.015.

References

Adrover, M., Farrús, E., Moyà, G., Vadell, J., 2012. Chemical properties and biological activity in soils of Mallorca following twenty years of treated wastewater irrigation. J. Environ. Manag. 95, 188–192.
Assouline, S., Narkis, K., 2011. Effects of long-term irrigation with treated wastewater on the hydraulic properties of a clayey soil. Water Resour. Res. 47, W08530.
Bachmann, J., Ellies, A., Hartge, K.H., 2000. Development and application of a new sessile drop contact angle method to assess soil water repellency. J. Hydrol. 231-232, 66–75.
Bardhan, G., Russo, D., Goldstein, D., Levy, G., 2016. Changes in the hydraulic properties of a clay soil under long-term irrigation with treated wastewater. Geoderma 264, 1–9.
Bauters, T., Steenhuis, T., DiCarlo, D., Nieber, J., Dekker, L., Ritsema, C., Parlange, J.-Y., Haverkamp, R., 2000. Physics of water repellent soils. J. Hydrol. 231–232, 233–243.
Bedbabis, S., Ben Rouina, B., Boukhris, M., Ferrara, G., 2014. Effect of irrigation with treated wastewater on soil chemical properties and infiltration rate. J. Environ. Manag. 133, 45–50.
Diamantopoulos, E., Durner, W., Reszkowska, A., Bachmann, J., 2013. Effect of soil water

repellency on soil hydraulic properties estimated under dynamic conditions. J. Hydrol. 486, 175–186.
DIN ISO 11277, 2002. Soil Quality - Determination of Particle Size Distribution in Mineral Soil Material - Method by Sieving and Sedimentation. Beuth, Berlin.
Doerr, S.H., 1998. On standardizing the 'water drop penetration time' and the 'molarity of an ethanol droplet' techniques to classify soil hydrophobicity: a case study using medium textured soils. Earth Surf. Process. Landf. 23, 663–668.
Doube, M., Klosowski, M.M., Arganda-Carreras, I., Cordelières, F.P., Dougherty, R.P., Jackson, J.S., Schmid, B., Hutchinson, J.R., Shefelbine, S.J., 2010. Bonej: free and extensible bone image analysis in ImageJ. Bone 47, 1076–1079.
Elifantz, H., Kautsky, L., Mor-Yosef, M., Tarchitzky, J., Bar-Tal, A., Chen, Y., Minz, D., 2011. Microbial activity and organic matter dynamics during 4 years of irrigation with treated wastewater. Microb. Ecol. 62, 973–981.
Frenk, S., Hadar, Y., Minz, D., 2014. Resilience of soil bacterial community to irrigation with water of different qualities under Mediterranean climate. Environ. Microbiol. 16, 559–569.
Halliwell, D.J., Barlow, K.M., Nash, D.M., 2001. A review of the effects of wastewater sodium on soil physical properties and their implications for irrigation systems. Soil Res. 39, 1259–1267.
Ibekwe, A.M., Gonzalez-Rubio, A., Suarez, D.L., 2018. Impact of treated wastewater for irrigation on soil microbial communities. Sci. Total Environ. 622-623, 1603–1610.
Jahn, R., Blume, H.P., Asio, V.B., Spaargaren, O., Schad, P., 2006. Guidelines for Soil Description, 4th edition. FAO, Rome.
Jueschke, E., Marschner, B., Tarchitzky, J., Chen, Y., 2008. Effects of treated wastewater irrigation on the dissolved and soil organic carbon in Israeli soils. Water Sci. Technol. 57, 727–733.
Kuka, K., Illerhaus, B., Fritsch, G., Joschko, M., Rogasik, H., Paschen, M., Schulz, H., Seyfarth, M., 2013. A new method for the extraction of undisturbed soil samples for X-ray computed tomography. J. Nondestruct. Test. 8.
Lado, M., Bar-Tal, A., Azenkot, A., Assouline, S., Ravina, I., Erner, Y., Fine, P., Dasberg, S., Ben-Hur, M., 2012. Changes in chemical properties of semiarid soils under long-term secondary treated wastewater irrigation. Soil Sci. Soc. Am. J. 76, 1358–1369.
Lado, M., Ben-Hur, M., 2009. Treated domestic sewage irrigation effects on soil hydraulic properties in arid and semiarid zones: a review. Soil Tillage Res. 106, 152–163.
Lado, M., Ben-Hur, M., 2010. Effects of irrigation with different effluents on saturated hydraulic conductivity of arid and semiarid soils. Soil Sci. Soc. Am. J. 74, 23–32.
Lado, M., Ben-Hur, M., Assouline, S., 2005. Effects of effluent irrigation on seal formation, infiltration, and soil loss during rainfall. Soil Sci. Soc. Am. J. 69, 1432–1439.
Lenth, R.V., 2016. Least-squares means: the R package lsmeans. J. Stat. Softw. 69, 1–33.
Leuther, F., Weller, U., Wallach, R., Vogel, H.-J., 2018. Quantitative analysis of wetting front instabilities in soil caused by treated waste water irrigation. Geoderma 319, 132–141.
Levy, G.J., 2011. Impact of long-term irrigation with treated wastewater on soil-structure stability - the Israeli experience. Isr. J. Plant Sci. 59, 95–104.
Marschner, H., Römheld, V., Horst, W.J., Martin, P., 1986. Root-induced changes in the rhizosphere: importance for the mineral nutrition of plants. Z. Pflanzenernaehr. Bodenkd. 149, 441–456.
Mevik, B.-H., Wehrens, R., 2007. The pls package: principal component and partial least squares regression in R. J. Stat. Softw. 18, 1–23.
Oades, J.M., 1993. The role of biology in the formation, stabilization and degradation of soil structure. Geoderma 56, 377–400.
OECD, 2015. Water Resources Allocation: Sharing Risks and Opportunities. OECD Publishing, Paris.
Pedrero, F., Kalavrouziotis, I., Alarcón, J.J., Koukoulakis, P., Asano, T., 2010. Use of treated municipal wastewater in irrigated agriculture - review of some practices in Spain and Greece. Agric. Water Manag. 97, 1233–1241.
Rahav, M., Brindt, N., Yermiyahu, U., Wallach, R., 2017. Induced heterogeneity of soil water content and chemical properties by treated wastewater irrigation and its reclamation by freshwater irrigation. Water Resour. Res. 53, 4756–4774.
Renard, P., Allard, D., 2013. Connectivity metrics for subsurface flow and transport. Adv. Water Resour. 51, 168–196.
Rengasamy, P., 2010. Soil processes affecting crop production in salt-affected soils. Funct. Plant Biol. 37, 613–620.
Rowell, D.L., 1994. Soil Science: Methods and Applications. Harlow Longman Scientific & Technical, London.
Schacht, K., Marschner, B., 2015. Treated wastewater irrigation effects on soil hydraulic conductivity and aggregate stability of loamy soils in Israel. J. Hydrol. Hydromech. 63, 47–54.
Schindelin, J., Arganda-Carreras, I., Frise, E., Kaynig, V., Longair, M., Pietzsch, T., Preibisch, S., Rueden, C., Saalfeld, S., Schmid, B., Tinevez, J.-Y., White, D.J., Hartenstein, V., Eliceiri, K., Tomancak, P., Cardona, A., 2012. Fiji: an open-source platform for biological-image analysis. Nat. Methods 9, 676–682.
Schindler, U., Durner, W., von Unold, G., Müller, L., 2010. Evaporation method for measuring unsaturated hydraulic properties of soils: extending the measurement range. Soil Sci. Soc. Am. J. 74, 1071–1083.
Schlüter, S., Leuther, F., Vogler, S., Vogel, H.J., 2016. X-ray microtomography analysis of soil structure deformation caused by centrifugation. Solid Earth 7, 129–140.
Schlüter, S., Sheppard, A., Brown, K., Wildenschild, D., 2014. Image processing of multiphase images obtained via X-ray microtomography: a review. Water Resour. Res. 50, 3615–3639.
Singer, A., 2007. The Soils of Israel. Springer-Verlag Berlin Heidelberghttps://doi.org/10.1007/978-3-540-71734-8.
Tarchouna, L.G., Merdy, P., Raynaud, M., Pfeifer, H.-R., Lucas, Y., 2010. Effects of long-term irrigation with treated wastewater. Part I: evolution of soil physico-chemical properties. Appl. Geochem. 25, 1703–1710.
Vogel, H.J., Weller, U., Schlüter, S., 2008. Quantim- c/c++ library for scientific image processing. http://www.quantim.ufz.de (accessed 15 May 2017).
Vogel, H.J., Weller, U., Schlüter, S., 2010. Quantification of soil structure based on Minkowski functions. Comput. Geosci. 36, 1236–1245.
Wallach, R., Ben-Arie, O., Graber, E.R., 2005. Soil water repellency induced by long-term irrigation with treated sewage effluent. J. Environ. Qual. 34, 1910–1920.
Wallach, R., Jortzick, C., 2008. Unstable finger-like flow in water-repellent soils during wetting and redistribution - the case of a point water source. J. Hydrol. 351, 26–41.
Weller, U., Vogel, H.J., 2012. Conductivity and hydraulic nonequilibrium across drainage and infiltration fronts. Vadose Zone J. 11.